iScience

Article

An $[Ag_3(dppy)_2(NO_3)_3]_n$ cluster polymer with narrowing fluorescence

Graphical abstract

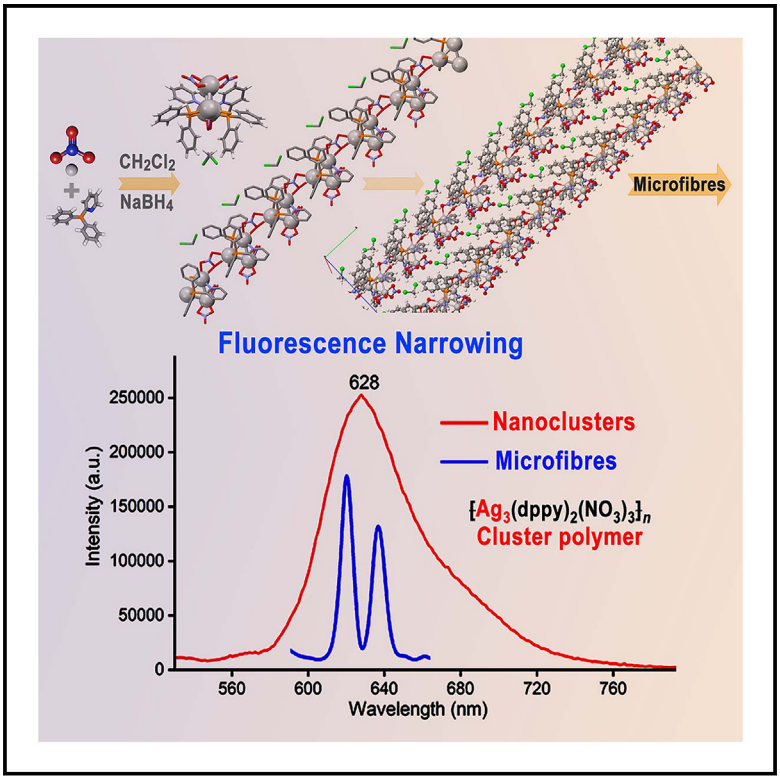

Highlights

- We report an innovative strategy in synthesizing a novel $[Ag_3(dppy)_2(NO_3)_3]_n$ cluster polymer
- The $[Ag_3(dppy)_2(NO_3)_3]_n$ cluster polymer demonstrates multicolor emissions
- We have synthesized microfibers of this cluster polymer by a facile precipitation technique
- The microfibers of this cluster polymer exhibit significant fluorescence emission narrowing

Authors

Blessing D. Peter, Qiuhao Yi, Chaonan Cui, Andrea Biffis, Jiannian Yao, Zhixun Luo

Correspondence

zxluo@iccas.ac.cn

In brief

Nanocomplex; Chemical synthesis; Nanomaterials; Optical property

Peter et al., 2025, iScience *28*, 111982
March 21, 2025
https://doi.org/10.1016/j.isci.2025.111982

CellPress

iScience

CellPress
OPEN ACCESS

Article

An $[Ag_3(dppy)_2(NO_3)_3]_n$ cluster polymer with narrowing fluorescence

Blessing D. Peter,[1,2,5] Qiuhao Yi,[1,2,5] Chaonan Cui,[1] Andrea Biffis,[3] Jiannian Yao,[1,4] and Zhixun Luo[1,2,6,*]

[1]Beijing National Laboratory for Molecular Sciences (BNLMS), State Key Laboratory for Structural Chemistry of Unstable and Stable Species, Institute of Chemistry, Chinese Academy of Sciences, Beijing 100190, China

[2]School of Chemical Science, University of Chinese Academy of Sciences, Beijing 100049, China

[3]Dipartimento di Scienze Chimiche, Universita degli Studi di Padova, 35131 Padova, Italy

[4]Laboratory of Photochemistry, Institute of Chemistry, Chinese Academy of Sciences, Beijing 100190, China

[5]These authors contributed equally

[6]Lead contact

*Correspondence: zxluo@iccas.ac.cn

https://doi.org/10.1016/j.isci.2025.111982

SUMMARY

Low-dimensional nanomaterials with lattice confinement, including those of nanoclusters (NCs), offer benefits for fluorescence narrowing. Compared to quantum dots of metal NCs, however, one-dimensional structures of such NCs challenge the single-crystal synthesis. Here, we report the synthesis of a novel $[Ag_3(dppy)_2(NO_3)_3]_n$ cluster polymer through the reduction of $AgNO_3$ with $NaBH_4$ in a dark environment. This cluster polymer incorporates the coordination and passivation of both diminished nitro groups (NO_3) and diphenyl-2-pyridylphosphine (dppy) ligands. The weak Ag-Ag metallic bonds within this cluster polymer are governed by argentophilic interactions, with each Ag_3 unit connected by a NO_3 group. This cluster polymer exhibits photoluminescence with three emission bands at 308, 352, and 620 nm, aligned with the purple (308/352 nm) and red (620 nm) regions, respectively. We synthesized microfibers of this cluster polymer using reprecipitation, resulting in a fluorescence bandwidth reduction to approximately one-tenth in the microfiber samples relative to the diluted solution.

INTRODUCTION

A variety of fluorescent nanomaterials have been developed, primarily comprising rare-earth complexes, inorganic quantum dots, and small organic molecules and organic polymers. These nanomaterials hold significant promise for applications in chemical sensors, data encryption, bioimaging, drug delivery, light-emitting diodes (LEDs), etc.[1–3] The evaluation of their optical properties largely hinges on color purity, which can be assessed by measuring the full width at half-maximum (FAHM) of the emission spectra.[4–8] Emissions with a narrow bandwidth are essential for this evaluation. Recently, narrow-bandwidth luminophores with high color purity have gained attention for their roles in critical fields such as information monitoring and photoelectric displays. However, the practical application of luminophores is often constrained by challenges related to stability and toxicity.[9,10]

Recent research to achieve narrowband luminescence has focused on organic molecule strategies. However, π-conjugated organic fluorophores may bear limited color purity due to broad emission spectra. It was found that the use of twisted or rigid structures with fused aromatic backbones led to substantial narrowband emissions.[11] For example, Anthony et al.[12] reported the synthesis of a tetracene derivative of stiff structure, showing narrowband emission suitable for hyperfluorescent organic LEDs. Kotwica et al.[13] studied the thermally activated delayed fluorescence and found that narrowband fluorescent dopants can attain elevated external quantum efficiency and color purity. Park et al.[14] developed a variety of narrow blue-emitting fluorophores allowing to inhibit aggregation-caused quenching.[1,15] Zhao et al.[16] illustrated that the reduction of fluorescence bandwidth can be influenced by four factors, including quantum confinement effect, surface state, molecular state, and cross-linkers.[17] Low-dimensional nanomaterials, including fluorescent quantum dots and chain structures like microfibers, offer benefits for fluorescence narrowing due to lattice confinement, which is based on distinctive geometric configuration and uniform molecule orientation.[18]

While currently engaging in fewer investigations, one-dimensional cluster polymers are anticipated to attract reasonable research interest in fluorescence narrowing. Atomically precise metal clusters have been extensively investigated,[19–25] and the luminosity of some nanoclusters (NCs) could surpass that of conventional fluorescent materials.[26–44] A few studies have shown the formation of coordination oligomers from these NCs,[45–51] elucidating the origin of novel properties and the relationship with the multi-level cluster structures. Here, we report the synthesis of a fluorescent cluster polymer $[Ag_3(dppy)_2(NO_3)_3]_n$ by a facile one-pot method. Based on this cluster polymer, we have prepared one-dimensional microfibers via the

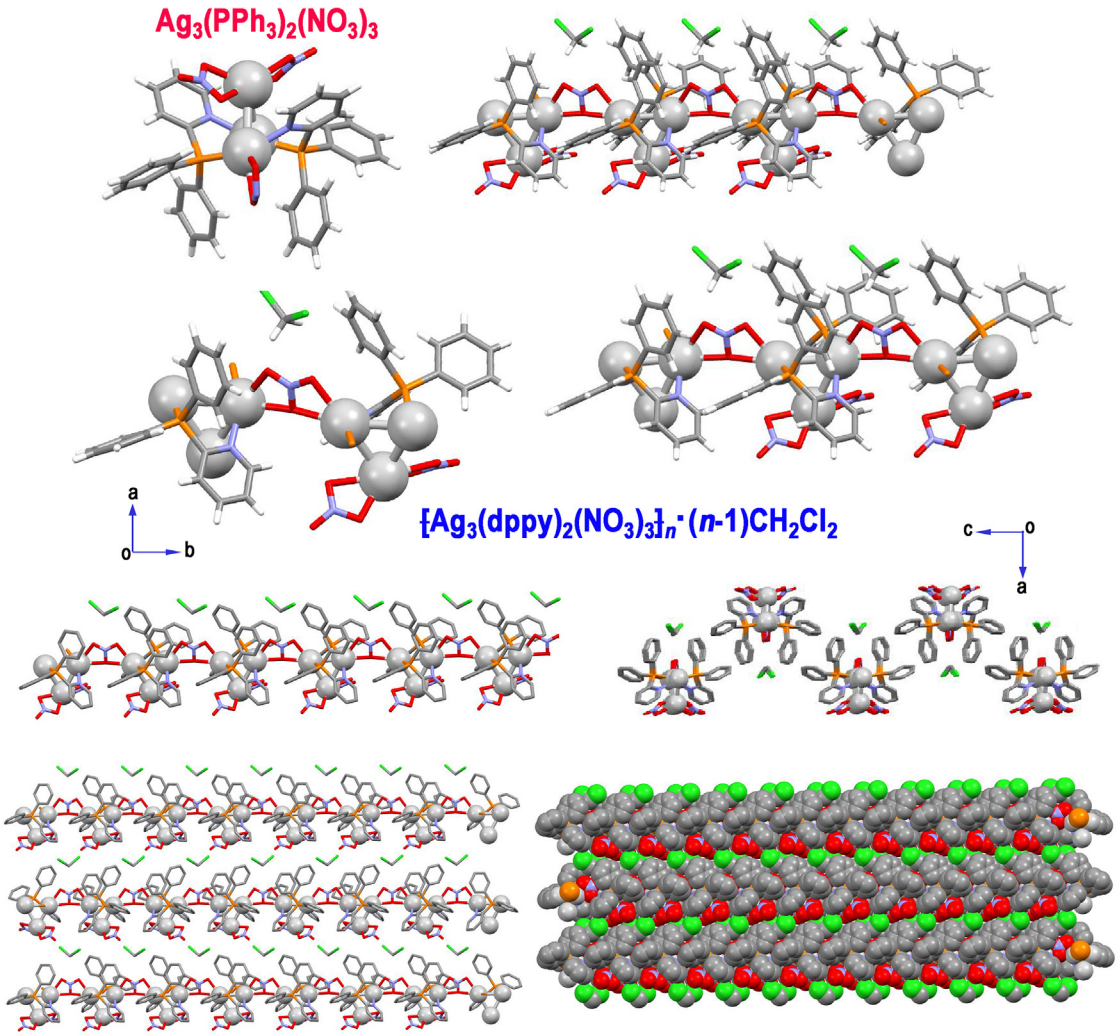

Figure 1. Single-crystal parsing of the $[Ag_3(dppy)_2(NO_3)_3]_n$ cluster polymer
The chemical structures of the monomer, dimer and trimer, tetramer, pentamer, hexamer, and three-dimensional packing are displayed.

reprecipitation technique, exhibiting notable fluorescence narrowing features.

RESULTS

The synthesis and characterization

Single-crystal X-ray diffraction (XRD) was utilized to characterize the $[Ag_3(dppy)_2(NO_3)_3]_n$ cluster polymer. The crystallographic analysis revealed that the single crystal exhibits an orthorhombic syngony and is classified within the Pcca space group (Table S1). As shown in Figure 1, the basic unit of this cluster polymer consists of three interconnected Ag atoms forming a triangular facet. One of the three silver atoms is passivated by two bidentate nitrate moieties, while the other two silver atoms are protected by two diphenyl-2-pyridylphosphine (dppy) ligands and each is coupled to an adjacent Ag_3 monomer through a nitrate linker. This cluster polymer exemplifies the mixed coordination of both organic and inorganic hybrid ligands.

As illustrated in Figure 1, the dimer, trimer, tetramer, etc., with a CH_2Cl_2 solvent molecule being interspersed between each monomer, present a regular formula of $[Ag_3(dppy)_2(NO_3)_3]_n \cdot (n\text{-}1)CH_2Cl_2$. The mean Ag-Ag distance was roughly 3.12 Å, which is within twice of the van der Waals radius of Ag, indicating that the spatial configuration of Ag atoms is influenced by argentophilic interaction. The lattice packing demonstrates the construction of an elongated chain of the $[Ag_3(dppy)_2(NO_3)_3]_n$ cluster polymer in the (101) and (011) directions (Figure S1), signifying the reduction of silver ions in competition with dppy coordination and polymerization along the -Ag-Ag- chain; meanwhile, this is accompanied by another $-Ag(NO_3)_2$ moiety at the side position. Every two Ag_3 units are linked by a NO_3 group to form the cluster polymer $[Ag_3(dppy)_2(NO_3)_3]_n$. Notably, the chain packing of cluster polymer is distinct from the cluster assembly obtained by introducing Ag-O, Ag-S, or Ag-Cl linkers into pre-formed NCs.[42] Also, this differs from significant prior studies of phosphine- and diphosphine-protected

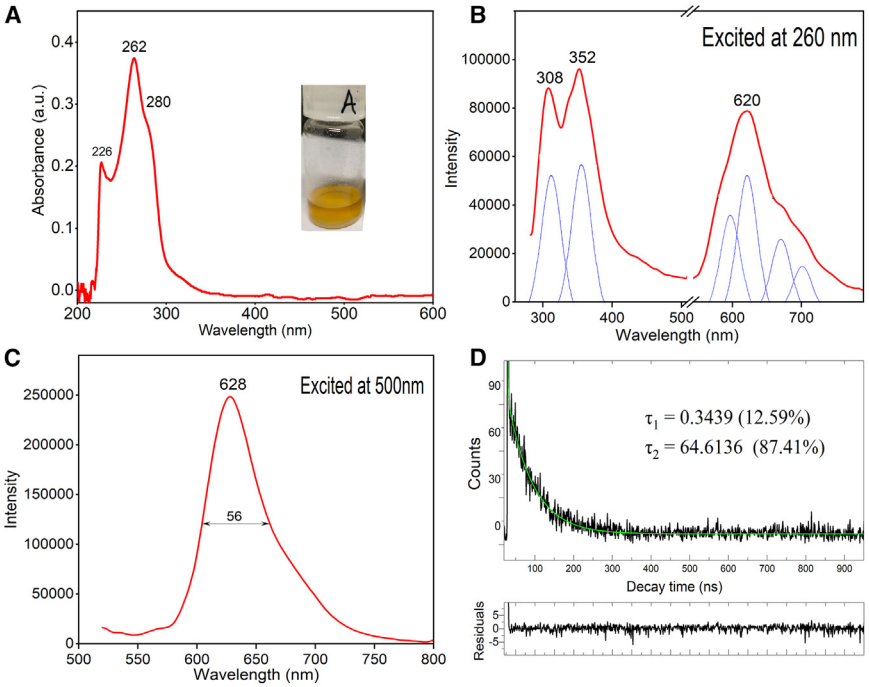

Figure 2. Optical properties of the $[Ag_3(dppy)_2(NO_3)_3]_n$ cluster polymer

(A) UV-vis absorption spectrum of $[Ag_3(dppy)_2(NO_3)_3]_n$.

(B and C) Emission spectra of the $[Ag_3(dppy)_2(NO_3)_3]_n$ cluster excited at 260 nm and 500 nm, respectively. The sample of 0.6 μL cluster was dissolved in 1 mL dichloromethane solvent. The light blue curves are based on Gaussian linear fitting; the peak values and FWHM are labeled.

(D) The decay of fluorescence emission at 628 nm of the $[Ag_3(dppy)_2(NO_3)_3]_n$ clusters, with a fitting curve shown in green, and the residual deviation given below the decay curve.

gold clusters having NO_3^- moieties, such as $Au_8(PPh_3)_8(NO_3)_2$,[52] $Au_9(PPh_3)_8(NO_3)_2$, and $Au_{14}(PPh_3)_6(NO_3)_4$,[53] as well as $Au_6(PPh_3)_6(NO_3)_2$ and $Au_6(dppp)_4(NO_3)_2$ (dppp = 1,3-bis(diphenylphosphino)-propane).[54] These gold clusters conform to the conventional monomeric structure of metal cluster complexes, with no detectable role of the nitrate anions as ligands. This is attributable to the distinct local interactions, coordination, and crystal growth mechanisms of gold and silver NCs.

Figure 2 illustrates the UV-vis and fluorescence spectra of the $[Ag_3(dppy)_2(NO_3)_3]_n$ cluster polymers. The ultraviolet-visible (UV-vis) absorption spectrum in CH_2Cl_2 solution reveals a characteristic peak in the 200 to 900 nm range, featuring a prominent band at 262 nm and two shoulder peaks at 226 nm and 280 nm(Figure 2A). These optical absorption peaks are assigned to the electronic transition involving dominant contributions from the dppy ligand. We measured ^{1}H-NMR of the $[Ag_3(dppy)_2(NO_3)_3]_n$ cluster in a comparison with that of the ligand dppy (Figure S2). It is found that the presence of Ag_3 and NO_3 in the cluster does not bring forth significant changes to the NMR signal of the original CH_x groups but somewhat alters their chemical shifts. Also, X-ray photoelectron spectroscopy (XPS) spectrum (Figure S3) of Ag 3d display two peaks at binding energy values of 368.51 eV and 374.67 eV, corresponding to Ag $3d_{5/2}$ and Ag $3d_{3/2}$, respectively, at the valence state of Ag(0). It is worth mentioning that the Ag−O bond length in this cluster polymer is up to 2.59 Å (Table S2), which is significantly larger than the normal value in the $AgNO_3$ compound.

We then examined the photoluminescence of this cluster polymer and observed multiple emission bands at 308/352 nm and 620 nm (Figure 2B), corresponding to the purple and red regions, respectively. Dual and triple emissions were frequently reported in ligand-protected metal clusters, resulting from the radiation of highly excited states within and against Kasha's rule.[55–61] Various emissions produce unique fingerprints that can be employed for ratiometric fluorescence sensing, allowing the evaluation of inhomogeneous parameters to be irrespective of external conditions.[62,63] We have also analyzed the red emission utilizing near-resonant excitation at 500 nm (Figure 2C) and observed that the peak exhibits a redshift to 628 nm, a slight narrowing of FWHM, likely associated with local interactions and quantum confinement effect, as well as the balance of radiative and non-radiative decay channels. Also observed is a substantial increase in intensity. Notably, fluorescence lifetime measurements showed that the emission at 628 nm has a dominant decay lifetime of 64.6 ns (Figure 2D), indicative of normal fluorescence emission characteristics pertaining to the deexcitation of S_1 to S_0 according to Kasha's rule.

Preparation of the microfibers

In addition to analyzing the $[Ag_3(dppy)_2(NO_3)_3]_n$ cluster polymer, we prepared microfibers by injecting its saturated acetonitrile solutions into ice-cold water.[64] Figures 3A and 3B display the scanning electron microscopy (SEM) images of the synthesized microfibers, with diameters of a few microns and lengths up to dozens of micrometers (more details in Figures S5−S8). Figure 3C displays the XRD patterns of the single crystals and microfibers of the cluster polymer $[Ag_3(dppy)_2(NO_3)_3]_n$. The single-crystal sample exhibits distinct dual diffraction peaks at $2\theta = 8.8°$ (102) and 8.6° (200), while the microfibers display a slightly shifted diffraction peak at $2\theta = 9.4°$, suggesting that the microfibers predominantly preserve the cluster structure during the recrystallization process. $[Ag_3(dppy)_2(NO_3)_3]_n$ is non-planar and does not align with a (100) or (111) direction; instead, it exhibits chain structure along the favored (102) orientation.

Further, we have examined the photoluminescence of the microfibers to confirm the fluorescence narrowing effect. The microscope images (Figures 4C–4E) illustrate that these microfibers are luminescent, whereas the 620-nm emission displays two peaks with fluctuations in relative intensity at different

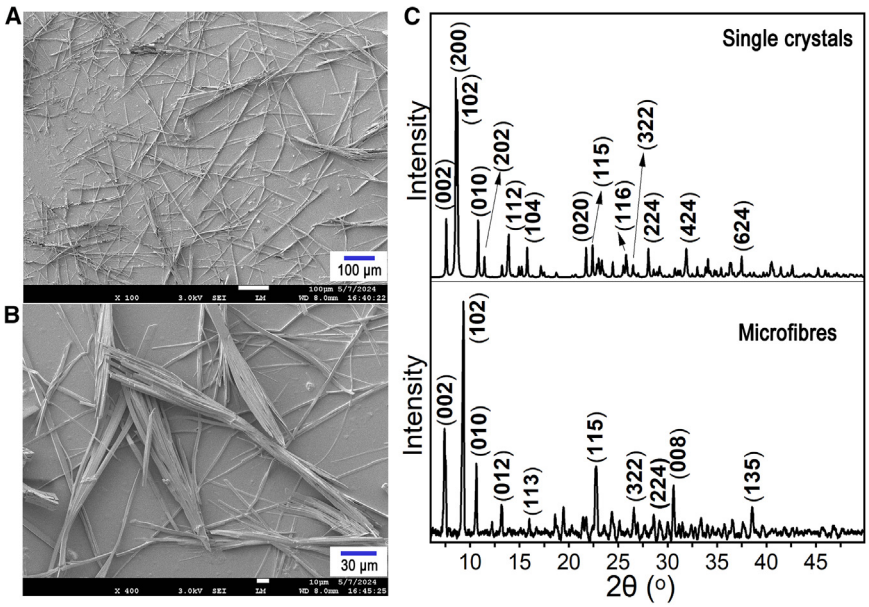

Figure 3. Morphology and XRD characterization

(A and B) SEM images of the microfibers by injecting saturated acetonitrile solution of $[Ag_3(dppy)_2(NO_3)_3]_n$ clusters into cold water.

(C) XRD patterns of the cluster single crystals and as-prepared microfibers.

measurement sites. This is in contrast with the single-crystal solution sample (Figure S4), which exhibits a peak at 628 nm by both a conventional spectrofluorometer and confocal microscopy. Notably, the microfibers of this cluster polymer cause fluorescence narrowing, showing FWHM values of 6 and 7 nm at the 598-nm and 614-nm emissions, respectively. Significant fluorescence narrowing phenomenon from $[Ag_3(dppy)_2(NO_3)_3]_n$ cluster polymer microfibers increases their applicability in luminescent devices and chemosensing.

The fundamental mechanism of unique emissions from this cluster polymer may be adjacent to the aggregation-induced emission effect typically due to the restriction of intramolecular motions.[65] Here, the cluster polymer states may inhibit intracluster vibrations and rotations, diminishing π-π interactions of the ligands and reducing non-radiative decay consequently. The electronic orbital energy levels in small NCs are discrete, with reasonable quantum confinement, and metal-metal bonding interactions sustain excited states and facilitate specific emission channels.

DFT calculations and hole-electron analysis

To clarify the origin of distinctive optical property of the $[Ag_3(dppy)_2(NO_3)_3]_n$ cluster polymer, we simulated the optical properties of the monomer and dimer via time-dependent density functional theory (TD-DFT) calculations. Figures 5A and 5B present the Kohn-Sham orbital energy level diagrams of an $Ag_3(dppy)_2(NO_3)_3$ monomer and its dimer, where the electronic transitions near the frontier orbitals are labeled (gray lines). Notably, the highest occupied molecular orbital (HOMO)-lowest unoccupied molecular orbital (LUMO) gap of the dimer is apparently smaller, indicating its first excitation state at a relatively lower energy. Considering that the orbital energy gap is not a direct correspondence of the excitation energy due to the missing Coulomb and exchange integrals between the occupied and virtual orbitals, we employed the Multiwfn software to conduct hole-electron analysis,[66,67] endeavoring to better understand the electronic excitations and unique optical property. The calculated absorption spectra reveal multiple distinct peaks, including 227, 262, and 279 nm, which are consistent with the experimental results although the relative absorbance intensities show significant variance likely due to the solvent effect or ambient conditions. Notably, the calculated UV-vis spectrum of an $Ag_3(dppy)_2(NO_3)_3$ monomer (Figure 5C) exhibits several peaks between 350 and 500 nm, whereas the spectrum of the dimer (Figure 5D) shows weakened intensity with minor redshifts in the low-energy region. These peaks are anticipated to diminish progressively as the Ag_3 unit elongates into a long chain, aligning with the experimental spectrum illustrated in Figure 2A.

A comparison of the calculated absorption spectra of the $Ag_3(dppy)_2(NO_3)_3$ monomer and its dimer is also conducted by the hole-electron analysis. It is shown that the ligand redistribution (red curves) constitutes the predominant contribution to the overall electronic spectra, succeeded by charge transfer from the ligand to the metal (Tables S4 and S5). This suggests that UV-vis absorption of this cluster polymer is governed by inherent characteristics of the ligands. The electron distribution in the dppy ligand resides on the aromatic rings, while the hole distribution predominantly occurs on the oxygen atoms of the nitrate ligand. This signifies that electrons are transported from the electron-rich nitrate ligand to the dppy ligand. The charge transfer spectra of the monomer and dimer are significantly similar, suggesting that the fundamental Ag_3 unit remains unchanged during polymer formation. This is consistent with the analysis of the infrared absorption spectra, which show that the microfibers retain the intrinsic structure of the nascent clusters (Figure S9; Table S3).

A minor alteration in the hole-electron analysis suggests that the fixed bridging nitrate ligand acts as an electron acceptor and exhibits distinct excitation properties relative to other free nitrate ligands (as electron donor). Conversely, the dppy ligand acts as an electron acceptor, allowing the bridging nitrate ligand to donate electrons and obtain a hole during excitation. The consistent charge transfer within the $[Ag_3(dppy)_2(NO_3)_3]_n$ cluster polymer contributes to its distinctive excitation state features. Notably, the first, second, and third excitation states of the dimer are exclusively contributed by HOMO→LUMO (99.0%), HOMO→LUMO+1 (96.2%), and HOMO-1→LUMO (96.3%), which is in sharp contrast to that of the

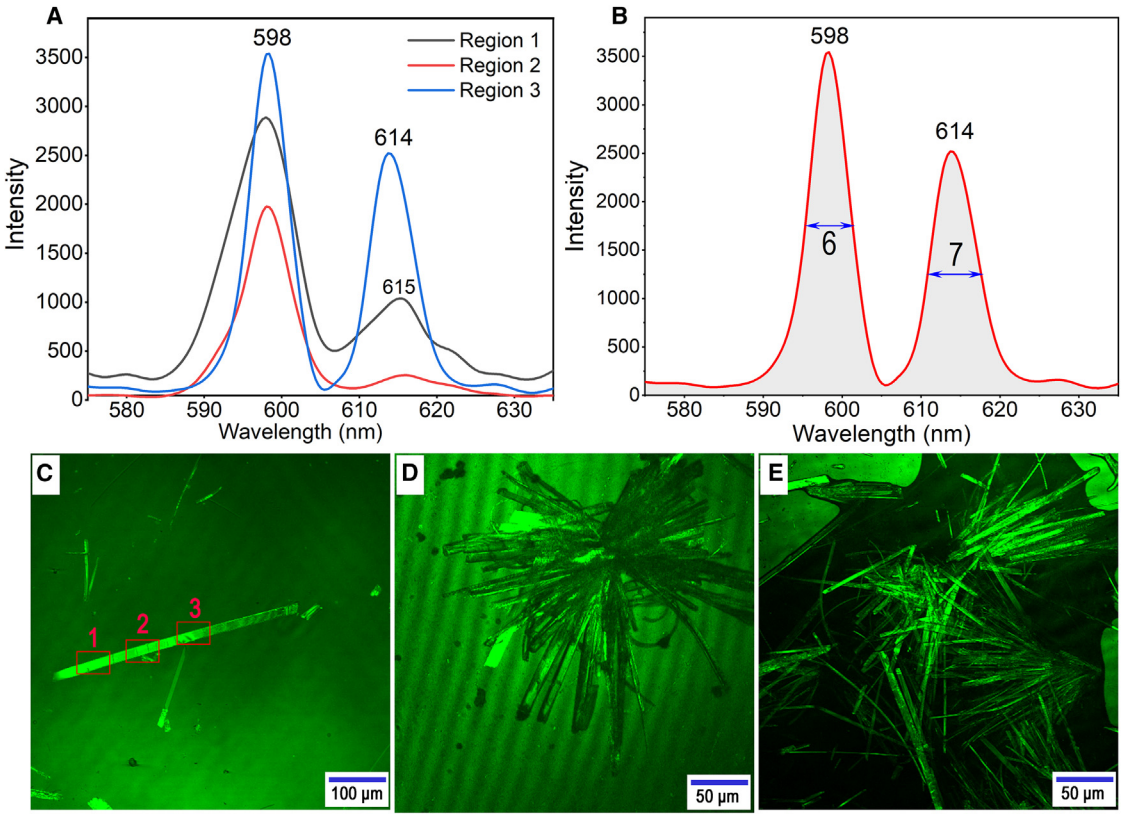

Figure 4. Confocal microfluorescence

(A and B) Fluorescence spectra of the microfiber samples of $[Ag_3(dppy)_2(NO_3)_3]_n$ clusters excited by a 559 nm laser.

(C–E) Photomicrographs of the microfibers. The red rectangles correspond to the different regions of the fluorescence measurements.

monomer where all the excitation states involve a mixture of multiple transitions (Table S4). It is thus inferred that, apart from the general principle within quantum confinement effect and ordered packing, the fluorescence narrowing of the microfibers is also associated with the chain structure of the cluster polymer.

DISCUSSION

We have synthesized a one-dimensional cluster polymer, $[Ag_3(dppy)_2(NO_3)_3]_n$, which exhibits triple emissions at 308 nm, 352 nm, and 620 nm. This finding demonstrates that the reduction of silver ions could compete with -Ag-Ag- chain polymerization within argentophilic interactions and dppy coordination, allowing the third Ag atom at the side position to be passivated by two NO_3 groups. Every two Ag_3 units are linked by a NO_3 group, yielding the $[Ag_3(dppy)_2(NO_3)_3]_n$ cluster polymer. Utilizing TD-DFT calculations and hole-electron analysis, we elucidated the reasonable stability and unique property of electronic states of the monomer and dimer. The distinctive -Ag-NO_3-Ag- linker, along with organic-inorganic ligand engineering, is essential in the formation of $[Ag_3(dppy)_2(NO_3)_3]_n$ polymer and contribute to the distinct emissions. By employing this cluster polymer, we produced microfibers using a precipitation method, resulting in notable reduction of fluorescence emission bandwidth. The one-pot strategy for this cluster polymer and microfibers is available for macroscale preparation.

Limitations of the study

This work demonstrates that the one-pot strategy for this cluster polymer and microfibers is available for macroscale preparation. However, we have not attained macroscale synthesis of this $[Ag_3(dppy)_2(NO_3)_3]_n$ cluster polymer for applications.

RESOURCE AVAILABILITY

Lead contact

Requests for further information and resources should be directed to and will be fulfilled by the lead contact, Zhixun Luo (zxluo@iccas.ac.cn).

Materials availability

All materials generated in this study are available from the lead contact without restriction.

Data and code availability

- The single-crystal structure reported in this article has been deposited in the Cambridge Crystallographic Data Center under accession number CCDC: 2383737. The NMR spectra in this study (Figure S2) has been deposited in Zenodo.org (https://doi.org/10.5281/zenodo.14791608).
- No code was generated in this study.

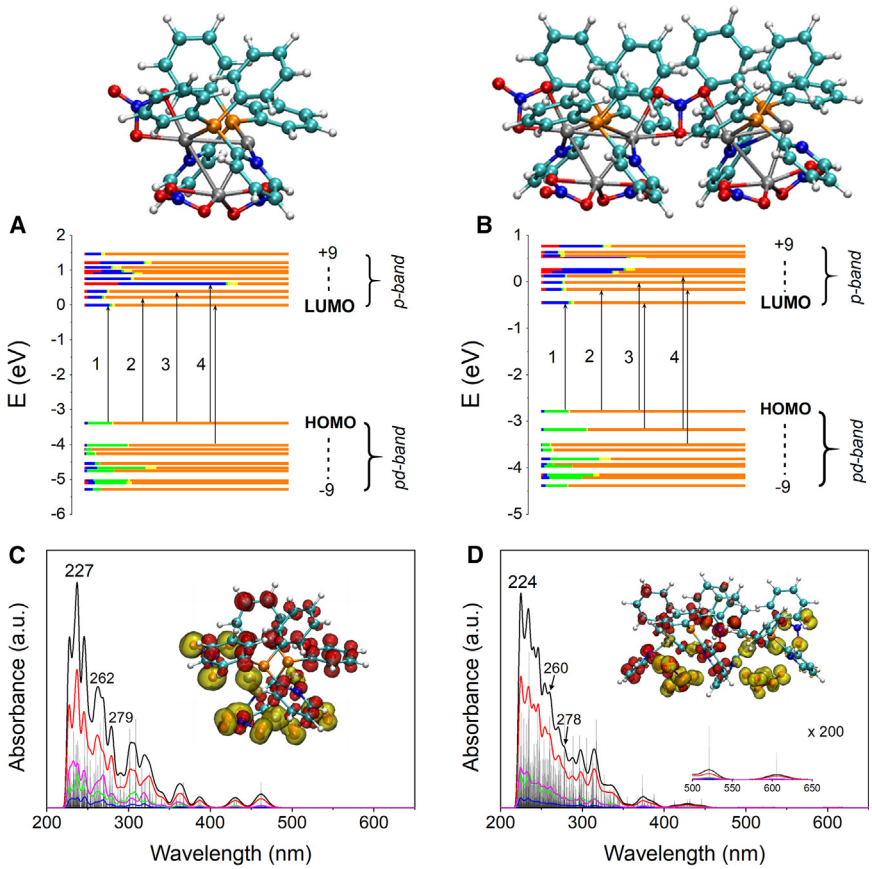

Figure 5. Molecular mechanism

(A and B) Kohn-Sham molecular orbital energy level diagrams of an $Ag_3(dppy)_2(NO_3)_3$ monomer and its dimer. Each orbital is drawn to indicate the relative contributions (given by the lengths of horizontal lines with color labels) of the atomic s (red), p (blue), and d (green) orbitals of Ag and s (yellow) and p (orange) orbitals of ligands. Vertical arrows indicate the electronic transitions near the frontier orbitals.

(C and D) TD-DFT computed UV-vis absorption spectra (black curves) of an $Ag_3(dppy)_2(NO_3)_3$ monomer and its dimer, along with hole-electron analysis showing the electronic excitation relating to redistribution of ligand (red curve), redistribution of metal (blue curves), electron transfer from metal to ligand (green curves), and electron transfer from ligand to metal (purple curves). The insets display the hole-electron distribution (yellow-red pattern) of corresponding excited states for the dominant peak in the UV-vis spectra.

- Any additional information required to reanalyze the data reported in this paper is available from the lead contact upon request.

ACKNOWLEDGMENTS

This work was supported by the Ministry of Science and Technology of the People's Republic of China (2020YFA0714602), the National Natural Science Foundation of China (grant no. 92261113), CAS Project for Young Scientists in Basic Research (grant no. YSBR-050), and CAS Key Research Program of Frontier Sciences (QYZDBSSW-SLH024).

AUTHOR CONTRIBUTIONS

Z.L. proposed the ideas and supervised the project. B.D.P. conducted the experiments. Q.Y. and C.C. performed the calculations. All authors contributed to the analysis and writing of the manuscript.

DECLARATION OF INTERESTS

The authors declare no competing interests.

STAR★METHODS

Detailed methods are provided in the online version of this paper and include the following:

SUPPLEMENTAL INFORMATION

Supplemental information can be found online at https://doi.org/10.1016/j.isci.2025.111982.

Received: December 24, 2024
Revised: January 22, 2025
Accepted: February 5, 2025
Published: February 10, 2025

REFERENCES

1. Thomas, S.W., Joly, G.D., and Swager, T.M. (2007). Chemical Sensors Based on Amplifying Fluorescent Conjugated Polymers. Chem. Rev. *107*, 1339–1386. https://doi.org/10.1021/cr0501339.
2. Li, D., Zhang, H., and Wang, Y. (2013). Four-coordinate organoboron compounds for organic light-emitting diodes (OLEDs). Chem. Soc. Rev. *42*, 8416–8433. https://doi.org/10.1039/c3cs60170f.
3. Xu, Y., Xu, P., Hu, D., and Ma, Y. (2021). Recent progress in hot exciton materials for organic light-emitting diodes. Chem. Soc. Rev. *50*, 1030–1069. https://doi.org/10.1039/d0cs00391c.
4. Ahn, D.H., Kim, S.W., Lee, H., Ko, I.J., Karthik, D., Lee, J.Y., and Kwon, J.H. (2019). Highly efficient blue thermally activated delayed fluorescence emitters based on symmetrical and rigid oxygen-bridged boron

acceptors. Nat. Photonics *13*, 540–546. https://doi.org/10.1038/s41566-019-0415-5.

5. Kotadiya, N.B., Blom, P.W.M., and Wetzelaer, G.-J.A.H. (2019). Efficient and stable single-layer organic light-emitting diodes based on thermally activated delayed fluorescence. Nat. Photonics *13*, 765–769. https://doi.org/10.1038/s41566-019-0488-1.

6. Tang, X., Cui, L.S., Li, H.C., Gillett, A.J., Auras, F., Qu, Y.K., Zhong, C., Jones, S.T.E., Jiang, Z.Q., Friend, R.H., and Liao, L.S. (2020). Highly efficient luminescence from space-confined charge-transfer emitters. Nat. Mater. *19*, 1332–1338. https://doi.org/10.1038/s41563-020-0710-z.

7. Abdurahman, A., Hele, T.J.H., Gu, Q., Zhang, J., Peng, Q., Zhang, M., Friend, R.H., Li, F., and Evans, E.W. (2020). Understanding the luminescent nature of organic radicals for efficient doublet emitters and pure-red light-emitting diodes. Nat. Mater. *19*, 1224–1229. https://doi.org/10.1038/s41563-020-0705-9.

8. Xiang, Y., Li, P., Gong, S., Huang, Y.-H., Wang, C.-Y., Zhong, C., Zeng, W., Chen, Z., Lee, W.-K., Yin, X., et al. (2020). Acceptor plane expansion enhances horizontal orientation of thermally activated delayed fluorescence emitters. Sci. Adv. *6*, eaba7855. https://doi.org/10.1126/sciadv.aba7855.

9. García de Arquer, F.P., Talapin, D.V., Klimov, V.I., Arakawa, Y., Bayer, M., and Sargent, E.H. (2021). Semiconductor quantum dots: Technological progress and future challenges. Science *373*, 640. https://doi.org/10.1126/science.aaz8541.

10. Dey, A., Ye, J., De, A., Debroye, E., Ha, S.K., Bladt, E., Kshirsagar, A.S., Wang, Z., Yin, J., Wang, Y., et al. (2021). State of the Art and Prospects for Halide Perovskite Nanocrystals. ACS Nano *15*, 10775–10981. https://doi.org/10.1021/acsnano.0c08903.

11. Ha, J.M., Hur, S.H., Pathak, A., Jeong, J.-E., and Woo, H.Y. (2021). Recent advances in organic luminescent materials with narrowband emission. NPG Asia Mater. *13*, 53. https://doi.org/10.1038/s41427-021-00318-8.

12. Odom, S.A., Parkin, S.R., and Anthony, J.E. (2003). Tetracene Derivatives as Potential Red Emitters for Organic LEDs. Org. Lett. *5*, 4245–4248. https://doi.org/10.1021/ol035415e.

13. Kotwica, K., Bujak, P., Data, P., Krzywiec, W., Wamil, D., Gunka, P.A., Skorka, L., Jaroch, T., Nowakowski, R., Pron, A., and Monkman, A. (2016). Soluble Flavanthrone Derivatives: Synthesis, Characterization, and Application to Organic Light-Emitting Diodes. Chem. Eur J. *22*, 7978–7986. https://doi.org/10.1002/chem.201600513.

14. Jung, H., Kang, S., Lee, H., Yu, Y.J., Jeong, J.H., Song, J., Jeon, Y., and Park, J. (2018). High Efficiency and Long Lifetime of a Fluorescent Blue-Light Emitter Made of a Pyrene Core and Optimized Side Groups. ACS Appl. Mater. Interfaces *10*, 30022–30028. https://doi.org/10.1021/acsami.8b09013.

15. Hong, Y., Lam, J.W.Y., and Tang, B.Z. (2009). Aggregation-induced emission: phenomenon, mechanism and applications. Chem. Commun. *7*, 4332–4353. https://doi.org/10.1039/b904665h.

16. Zhao, B., Ma, H., Zheng, M., Xu, K., Zou, C., Qu, S., and Tan, Z. (2022). Narrow-bandwidth emissive carbon dots: A rising star in the fluorescent material family. Carbon Energy *4*, 88–114. https://doi.org/10.1002/cey2.175.

17. Ai, L., Yang, Y., Wang, B., Chang, J., Tang, Z., Yang, B., and Lu, S. (2021). Insights into photoluminescence mechanisms of carbon dots: advances and perspectives. Sci. Bull. *66*, 839–856. https://doi.org/10.1016/j.scib.2020.12.015.

18. Zhao, Y.S., Fu, H., Peng, A., Ma, Y., Xiao, D., and Yao, J. (2008). Low-Dimensional Nanomaterials Based on Small Organic Molecules: Preparation and Optoelectronic Properties. Adv. Mater. *20*, 2859–2876. https://doi.org/10.1002/adma.200800604.

19. Luo, Z., Castleman, A.W., Jr., and Khanna, S.N. (2016). Reactivity of Metal Clusters. Chem. Rev. *116*, 14456–14492. https://doi.org/10.1021/acs.chemrev.6b00230.

20. Biffis, A., Centomo, P., Del Zotto, A., and Zecca, M. (2018). Pd Metal Catalysts for Cross-Couplings and Related Reactions in the 21st Century: A Critical Review. Chem. Rev. *118*, 2249–2295. https://doi.org/10.1021/acs.chemrev.7b00443.

21. Kang, X., Li, Y., Zhu, M., and Jin, R. (2020). Atomically precise alloy nanoclusters: syntheses, structures, and properties. Chem. Soc. Rev. *49*, 6443–6514. https://doi.org/10.1039/C9CS00633H.

22. Su, Y.-M., Ji, B.-Q., Wang, Z., Zhang, S.-S., Feng, L., Gao, Z.-Y., Li, Y.-W., Tung, C.-H., Sun, D., and Zheng, L.-S. (2021). Anionic passivation layer-assisted trapping of an icosahedral Ag_{13} kernel in a truncated tetrahedral Ag_{89} nanocluster. Sci. China Chem. *64*, 1482–1486. https://doi.org/10.1007/s11426-021-1025-8.

23. Tan, Y.-L., Yang, L., Yu, T.-C., Yu, H., Wang, X.-Y., Song, Y.-L., Niu, Z., and Lang, J.-P. (2021). Solvent-driven reversible transformation between electrically neutral thiolate protected Ag_{25} and Ag_{26} clusters. Sci. China Chem. *64*, 948–952. https://doi.org/10.1007/s11426-020-9952-x.

24. Zhang, S.-S., Liu, R.-C., Zhang, X.-C., Feng, L., Xue, Q.-W., Gao, Z.-Y., Tung, C.-H., and Sun, D. (2021). Core engineering of paired core-shell silver nanoclusters. Sci. China Chem. *64*, 2118–2124. https://doi.org/10.1007/s11426-021-1060-3.

25. Wang, Z., Li, M.-D., Shi, J.-Y., Su, H.-F., Liu, J.-W., Feng, L., Gao, Z.-Y., Xue, Q.-W., Tung, C.-H., Sun, D., and Zheng, L.-S. (2022). In Situ Capture of a Ternary Supramolecular Cluster in a 58-Nuclei Silver Supertetrahedron. CCS Chem. *4*, 1788–1795. https://doi.org/10.31635/ccschem.021.202100880.

26. Jin, R., Liu, C., Zhao, S., Das, A., Xing, H., Gayathri, C., Xing, Y., Rosi, N.L., Gil, R.R., and Jin, R. (2015). Tri-icosahedral Gold Nanocluster $[Au_{37}(PPh_3)_{10}(SC_2H_4Ph)_{10}X_2]^+$: Linear Assembly of Icosahedral Building Blocks. ACS Nano *9*, 8530–8536. https://doi.org/10.1021/acsnano.5b03524.

27. Jing, X., Fu, F., Wang, R., Xin, X., Qin, L., Lv, H., and Yang, G.Y. (2022). Robust Enantiomeric Two-Dimensional Assembly of Atomically Precise Silver Clusters. ACS Nano *16*, 15188–15196. https://doi.org/10.1021/acsnano.2c06492.

28. Liu, Q., He, S., Yu, B., Cheng, X., Shi, W., and Wang, X. (2022). Visible Light Induced Ag-Polyoxometalate Coassembly into Single-Cluster Nanowires. Adv. Mater. *34*, 2206178. https://doi.org/10.1002/adma.202206178.

29. Fan, X., Yuan, F., Li, D., Chen, S., Cheng, Z., Zhang, Z., Xiang, S., Zang, S.Q., Zhang, J., and Zhang, L. (2021). Threefold Collaborative Stabilization of Ag_{14}-Nanorods by Hydrophobic Ti_{16}-Oxo Clusters and Alkynes: Designable Assembly and Solid-State Optical-Limiting Application. Angew. Chem. Int. Ed. *60*, 12949–12954. https://doi.org/10.1002/anie.202101664.

30. Jin, Y., Li, S., Han, Z., Yan, B.J., Li, H.Y., Dong, X.Y., and Zang, S.Q. (2019). Cations Controlling the Chiral Assembly of Luminescent Atomically Precise Copper(I) Clusters. Angew. Chem. Int. Ed. *58*, 12143–12148. https://doi.org/10.1002/anie.201906614.

31. Santiago-Gonzalez, B., Monguzzi, A., Capitani, C., Prato, M., Santambrogio, C., Meinardi, F., and Brovelli, S. (2018). Bottom-up Synthesis and Self-Assembly of Copper Clusters into Permanent Excimer Supramolecular Nanostructures. Angew. Chem. Int. Ed. *57*, 7051–7055. https://doi.org/10.1002/anie.201801806.

32. Wu, H., He, X., Yang, B., Li, C.C., and Zhao, L. (2021). Assembly-Induced Strong Circularly Polarized Luminescence of Spirocyclic Chiral Silver(I) Clusters. Angew. Chem. Int. Ed. *60*, 1535–1539. https://doi.org/10.1002/anie.202008765.

33. Wu, Z., Du, Y., Liu, J., Yao, Q., Chen, T., Cao, Y., Zhang, H., and Xie, J. (2019). Aurophilic Interactions in the Self-Assembly of Gold Nanoclusters into Nanoribbons with Enhanced Luminescence. Angew. Chem. Int. Ed. *58*, 8139–8144. https://doi.org/10.1002/anie.201903584.

34. Liu, Q., and Wang, X. (2022). Fabricating sub-nanometer materials through cluster assembly. Chem. Sci. *13*, 12280–12289. https://doi.org/10.1039/d2sc03813g.

35. Wei, X., Kang, X., Yuan, Q., Qin, C., Jin, S., Wang, S., and Zhu, M. (2019). Capture of Cesium Ions with Nanoclusters: Effects on Inter- and Intramolecular Assembly. Chem. Mater. *31*, 4945–4952. https://doi.org/10.1021/acs.chemmater.9b01890.

36. Chen, X., Li, H.-X., Zhang, Z.-Y., Xu, C., Hou, K.-P., Zhou, L.-K., Lang, J.-P., and Sun, Z.-R. (2012). Assembly of two cluster-based coordination polymers with good NLO performance from one NLO-inactive precursor cluster. CrystEngComm *14*, 4027, $[Et_4N]$ $[Tp^*W(\mu_3\text{–}S)_3(CuCl)_3]$. https://doi.org/10.1039/c2ce25143d.

37. Zhou, K., Qin, C., Wang, X.-L., Shao, K.-Z., Yan, L.-K., and Su, Z.-M. (2014). Unexpected 1D self-assembly of carbonate-templated sandwich-like macrocycle-based $Ag_{20}S_{10}$ luminescent nanoclusters. CrystEngComm *16*, 7860. https://doi.org/10.1039/c4ce00867g.

38. Toniolo, D., Scopelliti, R., Zivkovic, I., and Mazzanti, M. (2020). Assembly of High-Spin $[Fe_3]$ Clusters by Ligand-Based Multielectron Reduction. J. Am. Chem. Soc. *142*, 7301–7305. https://doi.org/10.1021/jacs.0c01664.

39. Wang, Z.Y., Wang, M.Q., Li, Y.L., Luo, P., Jia, T.T., Huang, R.W., Zang, S.Q., and Mak, T.C.W. (2018). Atomically Precise Site-Specific Tailoring and Directional Assembly of Superatomic Silver Nanoclusters. J. Am. Chem. Soc. *140*, 1069–1076. https://doi.org/10.1021/jacs.7b11338.

40. Colliard, I., Morrison, G., Loye, H.C.Z., and Nyman, M. (2020). Supramolecular Assembly of U(IV) Clusters and Superatoms with Unconventional Countercations. J. Am. Chem. Soc. *142*, 9039–9047. https://doi.org/10.1021/jacs.0c03041.

41. Wu, Z., Liu, J., Gao, Y., Liu, H., Li, T., Zou, H., Wang, Z., Zhang, K., Wang, Y., Zhang, H., and Yang, B. (2015). Assembly-Induced Enhancement of Cu Nanoclusters Luminescence with Mechanochromic Property. J. Am. Chem. Soc. *137*, 12906–12913. https://doi.org/10.1021/jacs.5b06550.

42. Ebina, A., Hossain, S., Horihata, H., Ozaki, S., Kato, S., Kawawaki, T., and Negishi, Y. (2020). One-Two-and Three-Dimensional Self-Assembly of Atomically Precise Metal Nanoclusters. Nanomaterials *10*, 1105. https://doi.org/10.3390/nano10061105.

43. Li, Y., Zhou, M., Song, Y., Higaki, T., Wang, H., and Jin, R. (2021). Double-helical assembly of heterodimeric nanoclusters into supercrystals. Nature *594*, 380–384. https://doi.org/10.1038/s41586-021-03564-6.

44. Hau, S.C.K., Cheng, P.-S., and Mak, T.C.W. (2014). Ligand-Induced Assembly of Coordination Chains and Columns Containing High-Nuclearity Silver(I) Ethynide Cluster Units. Organometallics *33*, 3231–3234. https://doi.org/10.1021/om5003733.

45. Yang, X., Jones, R.A., and Huang, S. (2014). Luminescent 4f and d-4f polynuclear complexes and coordination polymers with flexible salen-type ligands. Coord. Chem. Rev. *273–274*, 63–75. https://doi.org/10.1016/j.ccr.2013.11.012.

46. De Nardi, M., Antonello, S., Jiang, D.-e., Pan, F., Rissanen, K., Ruzzi, M., Venzo, A., Zoleo, A., and Maran, F. (2014). Gold Nanowired: A Linear $(Au_{25})_n$ Polymer from Au_{25} Molecular Clusters. ACS Nano *8*, 8505–8512. https://doi.org/10.1021/nn5031143.

47. Tran, P.D., Tran, T.V., Orio, M., Torelli, S., Truong, Q.D., Nayuki, K., Sasaki, Y., Chiam, S.Y., Yi, R., Honma, I., et al. (2016). Coordination polymer structure and revisited hydrogen evolution catalytic mechanism for amorphous molybdenum sulfide. Nat. Mater. *15*, 640–646. https://doi.org/10.1038/nmat4588.

48. Liu, Q., Zhang, W.-H., and Lang, J.-P. (2017). Versatile thiomolybdate(thiotungstate)–copper–sulfide clusters and multidimensional polymers linked by cyanides. Coord. Chem. Rev. *350*, 248–274. https://doi.org/10.1016/j.ccr.2017.06.027.

49. Sengupta, T., Dang, T.T., Chung, J.S., and Kang, S.G. (2019). Insight into the structure and bonding of copper(i) iodide clusters and a cluster-based coordination polymer. New J. Chem. *43*, 16176–16187. https://doi.org/10.1039/c9nj02130b.

50. Wen, Z.-R., Guan, Z.-J., Zhang, Y., Lin, Y.-M., and Wang, Q.-M. (2019). $[Au_7Ag_9(dppf)_3(CF_3CO_2)_7BF_4]_n$: a linear nanocluster polymer from molecular Au_7Ag_8 clusters covalently linked by silver atoms. Chem. Commun. *55*, 12992–12995. https://doi.org/10.1039/C9CC05924E.

51. Kang, X.-M., Tang, M.-H., Yang, G.-L., and Zhao, B. (2020). Cluster/cage-based coordination polymers with tetrazole derivatives. Coord. Chem. Rev. *422*, 213424. https://doi.org/10.1016/j.ccr.2020.213424.

52. Gutrath, B.S., Schiefer, F., Homberger, M., Englert, U., Şerb, M.-D., Bettray, W., Beljakov, I., Meded, V., Wenzel, W., and Simon, U. (2016). Molecular and Electronic Structure of the Cluster $[Au_8(PPh_3)_8](NO_3)_2$. Eur. J. Inorg. Chem. *2016*, 975–981. https://doi.org/10.1002/ejic.201501334.

53. Gutrath, B.S., Oppel, I.M., Presly, O., Beljakov, I., Meded, V., Wenzel, W., and Simon, U. (2013). $Au_{14}(PPh_3)_8(NO_3)_4$: An Example of a New Class of $Au(NO_3)$-Ligated Superatom Complexes. Angew. Chem. Int. Ed. *52*, 3529–3532. https://doi.org/10.1002/anie.201208681.

54. Shichibu, Y., and Konishi, K. (2013). Electronic properties of [core+exo]-type gold clusters: factors affecting the unique optical transitions. Inorg. Chem. *52*, 6570–6575. https://doi.org/10.1021/ic4005592.

55. Xu, Q.Q., Dong, X.Y., Huang, R.W., Li, B., Zang, S.Q., and Mak, T.C.W. (2015). A thermochromic silver nanocluster exhibiting dual emission character. Nanoscale *7*, 1650–1654. https://doi.org/10.1039/c4nr05122j.

56. Anumula, R., Xiao, P., Cui, C., Wu, H., Cui, G., Fang, W.-h., Luo, Z., and Yao, J. (2020). A Small Bimetallic Ag_3Cu_2 Nanocluster with Dual Emissions within and against Kasha's Rule. Nanoscale *12*, 7864–7869. https://doi.org/10.1039/d0nr00471e.

57. Shan, X.-c., Jiang, F.-l., Yuan, D.-q., Zhang, H.-b., Wu, M.-y., Chen, L., Wei, J., Zhang, S.-q., Pan, J., and Hong, M.-c. (2013). A multi-metal-cluster MOF with Cu_4I_4 and Cu_6S_6 as functional groups exhibiting dual emission with both thermochromic and near-IR character. Chem. Sci. *4*, 1484–1489. https://doi.org/10.1039/C3SC21995J.

58. Zhang, X., Wu, X., Liu, X., Chen, G., Wang, Y., Bao, J., Xu, X., Liu, X., Zhang, Q., Yu, K., et al. (2020). Heterostructural $CsPbX_3$-PbS (X = Cl, Br, I) Quantum Dots with Tunable Vis–NIR Dual Emission. J. Am. Chem. Soc. *142*, 4464–4471. https://doi.org/10.1021/jacs.9b13681.

59. Behera, S.K., Park, S.Y., and Gierschner, J. (2021). Dual Emission: Classes, Mechanisms, and Conditions. Angew. Chem. Int. Ed. *60*, 22624–22638. https://doi.org/10.1002/anie.202009789.

60. Belau, L., Haas, Y., and Rettig, W. (2004). Dual Emission of 4-(1H-Pyrrol-1-yl)benzonitrile Clusters with Acetonitrile in a Supersonic. J. Phys. Chem. A *108*, 3916–3925. https://doi.org/10.1021/jp037547v.

61. Lei, Z., Guan, Z.J., Pei, X.L., Yuan, S.F., Wan, X.K., Zhang, J.Y., and Wang, Q.M. (2016). An Atomically Precise $Au_{10}Ag_2$ Nanocluster with Red–Near-IR Dual Emission. Chem. Eur J. *22*, 11156–11160. https://doi.org/10.1002/chem.201602403.

62. Shen, J.-Y., Chao, W.-C., Liu, C., Pan, H.-A., Yang, H.-C., Chen, C.-L., Lan, Y.-K., Lin, L.-J., Wang, J.-S., Lu, J.-F., et al. (2013). Probing water micro-solvation in proteins by water catalysed proton-transfer tautomerism. Nat. Commun. *4*, 2611. https://doi.org/10.1038/ncomms3611.

63. Wu, H., Anumula, R., Andrew, G.N., and Luo, Z. (2023). A stable superatomic $Cu_6(SMPP)_6$ nanocluster with dual emission. Nanoscale *15*, 4137–4142. https://doi.org/10.1039/d2nr07223h.

64. Luo, Z., Loo, B.H., Cao, X., Peng, A., and Yao, J. (2012). Probing the Conformational Transition of 2,2′-Bipyridyl under External Field by Surface-Enhanced Raman Spectroscopy. J. Phys. Chem. C *116*, 2884–2890. https://doi.org/10.1021/jp208566d.

65. Hong, Y., Lam, J.W.Y., and Tang, B.Z. (2011). Aggregation-induced emission. Chem. Soc. Rev. *40*, 5361–5388. https://doi.org/10.1039/c1cs15113d.

66. Liu, Z., Lu, T., and Chen, Q. (2020). An sp-hybridized all-carboatomic ring, cyclo[18]carbon: Electronic structure, electronic spectrum, and optical nonlinearity. Carbon *165*, 461–467. https://doi.org/10.1016/j.carbon.2020.05.023.

67. Lu, T., and Chen, F. (2012). Multiwfn: a multifunctional wavefunction analyzer. J. Comput. Chem. *33*, 580–592. https://doi.org/10.1002/jcc.22885.

68. Frisch, M.J., Trucks, G.W., Schlegel, H.B., Scuseria, G.E., Robb, M.A., Cheeseman, J.R., Scalmani, G., Barone, V., Petersson, G.A., Nakatsuji, H., et al. (2016). Gaussian 16 Rev. B.01 (Wallingford, CT).

69. Adamo, C., and Barone, V. (1999). Toward reliable density functional methods without adjustable parameters: The PBE0 model. J. Chem. Phys. *110*, 6158–6170. https://doi.org/10.1063/1.478522.

STAR★METHODS

KEY RESOURCES TABLE

REAGENT or RESOURCE	SOURCE	IDENTIFIER
Deposited data		
CCDC: 2383737	Single crystal	
https://doi.org/10.5281/zenodo.14791608	NMR	Figure S2

METHOD DETAILS

Materials

All of the chemicals and reagents were purchased from commercial sources and utilized without additional purification. These included silver nitrate ($AgNO_3$, 99.999%, Alfa Aesar), 2-(diphenylphosphine)pyridine (dppy, $C_{17}H_{14}NP$, 98%, Innochem), phenylacetylene (PhC≡C, C_8H_6, 98%, Innochem), sodium borohydride ($NaBH_4$, ≥98.0%, Sigma Aldrich), sodium chloride (NaCl), dichloromethane (DCM, CH_2Cl_2), acetonitrile (CH_3CN), and ethanol (EtOH, ≥99.8% Sigma-Aldrich).

Synthesis of $[Ag_3(dppy)_2(NO_3)_3]_n$

The synthesis of $[Ag_3(dppy)_2(NO_3)_3]_n$ was conducted by the following procedures. Initially, 28 mg solid silver nitrate ($AgNO_3$) was dissolved in 2 mL volume of ethanol with 5 min of sonication. The dppy ligand dissolved in dichloromethane (CH_2Cl_2, DCM) was incorporated into this solution and agitated for 30 min. Subsequently, 8 μL of phenylacetylene additive, 3.5 mg of NaOH in 0.5 mL of ethanol, and 10 mg of $NaBH_4$ reductant in 0.5 mL of ethanol were well mixed, and 70 μL of this mixture was applied to each sample. The reaction was sustained for 7 h with agitation under darkness. A greyish solution was obtained, indicating the formation of $[Ag_3(dppy)_2(NO_3)_3]_n$ cluster polymers. The solvent was then removed using rotary evaporation, and the resulting products were centrifuged at 1000 rpm and washed twice with methanol to remove excess ligands. Greyish crystals were grown in CH_2Cl_2 and n-hexane at 4°C for 14 days.

Synthesis of the microfibers

We prepared microfibers of the $[Ag_3(dppy)_2(NO_3)_3]_n$ cluster polymer by injecting its saturated acetonitrile solutions into ice-cold water.[64] Specifically, 1 mL acetonitrile solution of the cluster sample underwent sonication at 80°C in a water bath for 30 min, and was then then rapidly injected into test tube racks placed in ice-cold water. The sample was subsequently placed in a refrigerator at −4°C for 3 to 5 days to promote the growth into microfibers.[64] We tried diverse injection speed (c.a., 100 to 1000 μL/s) and concentrations to achieve uniform microfibers.

Characterization

The cluster structure was determined using single-crystal X-ray diffraction on an XtaLAB AFC10, analyzed with Olex2, refined by full-matrix least squares minimization, and anisotropically polished with all hydrogen atoms positioned geometrically. The morphology of microfibers was evaluated using various techniques, including field-emission scanning electron microscopy, high-resolution transmission electron microscopy, and X-ray photoelectron spectroscopy. The UV-Visible spectra of the cluster were acquired in the range of 200–800 nm using a Shimadzu UV-3600 spectrophotometer. Infrared spectra were acquired with an Avatar 330 FT-IR spectrometer, spanning the range of 4000−400 cm^{-1}, with KBr pellets. Fluorescence spectra were acquired using a Horiba Scientific Fluoromax-4 spectrofluorometer, by dissolving single crystals in DCM solvent. NMR spectra were acquired at ambient condition with a Bruker Magnet System functioning at 400 MHz/54 mm (Ultra Shield Plus), with chloroform as the solvent and tetramethylsilane as the internal standard. A laser scanning confocal microscope, Olympus Fluoview 1 × 81-FV 1000, was employed to get high-resolution images of the microfibers. The microscope employed 559 nm laser to excite the the microfibers.

Computational methods

The DFT calculations of the monomer and dimer were performed using the Gaussian 16 software,[68] employing the LANL2DZ basis set for Ag and the STO-3G basis set for nonmetal atoms (H, C, N, O, and P). The PBE0 hybrid functional was employed to predict the electronic structure and absorption spectrum of several ligand-protected Ag clusters by integrating 200–600 potential transitions.[69]

QUANTIFICATION AND STATISTICAL ANALYSIS

There are no quantification or statistical analyses to include in this study.